

International Journal of Modern Physics E
 © World Scientific Publishing Company

Core-crust transition properties of neutron stars within systematically varied extended relativistic mean-field model

A. Sulaksono

*Departemen Fisika, FMIPA, Universitas Indonesia,
 Depok, 16424, Indonesia*

Naosad Alam

Saha Institute of Nuclear Physics, Kolkata 700 064, India

B. K. Agrawal

Saha Institute of Nuclear Physics, Kolkata 700 064, India

Received (received date)

Revised (revised date)

The model dependence and the symmetry energy dependence of the core-crust transition properties for the neutron stars are studied using three different families of systematically varied extended relativistic mean field model. Several forces within each of the families are so considered that they yield wide variations in the values of the nuclear symmetry energy a_{sym} and its slope parameter L at the saturation density. The core-crust transition density is calculated using a method based on random-phase-approximation. The core-crust transition density is strongly correlated, in a model independent manner, with the symmetry energy slope parameter evaluated at the saturation density. The pressure at the transition point does not show any meaningful correlations with the symmetry energy parameters at the saturation density. At best, pressure at the transition point is correlated with the symmetry energy parameters and their linear combination evaluated at the some sub-saturation density. Yet, such correlations might not be model independent. The correlations of core-crust transition properties with the symmetry energy parameter are also studied by varying the symmetry energy within a single model. The pressure at the transition point is correlated once again with the symmetry energy parameter at the sub-saturation density.

Keywords: Neutron star; core-crust transition; symmetry energy.

PACS numbers:26.60.Gj; 21.30.Fe; 26.60.Kp

1. Introduction

The matter in the outer core of the neutron stars (NS) become unstable, against the density fluctuations, below a particular density so called core-crust transition density. The knowledge of the core-crust transition properties in NS matter is very important in understanding the pulsar glitches, crust relaxation in cooling and accreting neutron stars and asteroseismology from giant magnetar flares.¹ The values

of core-crust transition density and the corresponding pressure depend crucially on the behaviour of nuclear symmetry energy around the sub-saturation densities. However, density dependence of the nuclear symmetry energy is known with large uncertainties. Some progress in this direction has been made in the last few years.²⁻⁸ In the mean while, several investigations are carried out to study the effects of the variations in the symmetry energy on the core-crust transition properties. The variations in the symmetry energy were achieved either within a single model or by using large set of randomly selected models of different types. The core crust transition density is found to be strongly correlated with the various symmetry energy parameters evaluated at the saturation density. But, results for the correlations between the pressure at the transition point and the symmetry energy obtained from different investigations are at variance.

One usually considers the dependence of the core-crust transition properties on various nuclear symmetry energy parameters, like, symmetry energy coefficient a_{sym} and the slope parameter L ; the later characterizes the density dependence of the symmetry energy. It has been established that the core-crust transition density ρ_t is well correlated with L . However, the actual link between the pressure P_t , at the transition density, and L is rather uncertain. The calculations in Ref.⁹ were performed within a density dependent point coupling (DD-PC) model. Only a single accurately calibrated DD-PC model was used to study the correlations of the core-crust transition properties with the various quantities associated with the nuclear matter. The iso-scalar and iso-vector properties associated with nuclear matter were varied by changing the model parameters around their optimal values. In Ref.,¹⁰ a covariance analysis based on a single relativistic mean field (RMF) model was employed to study the correlations of various neutron star properties with the neutron-skin thickness in ^{208}Pb nucleus which is strongly correlated with the symmetry energy slope parameter L at the saturation density. In Ref,¹¹ several modified Gogny and commonly used Skyrme Hartree Fock (SHF) models were used to study the correlations between the core crust transition properties and the nuclear symmetry energy parameters. Both the ρ_t and P_t are found to be strongly correlated with L in Refs. ⁹⁻¹¹ The similar studies were performed in Ref.,¹² but, using appropriately calibrated several RMF and SHF models. The $\rho_t - L$ correlations were found to be strong, while, link between P_t and L was found to be sensitive to the models employed. The lack of $P_t - L$ correlations are attributed to the delicate balance between the contributions from the higher order terms and the shift in the transition density with L . The contributions from the higher order terms are model dependent. The P_t seemed to be better correlated with appropriate linear combination of L and the symmetry energy curvature parameter K_{sym} , both of these symmetry energy parameters were evaluated at a sub-saturation density. In particular, the P_t are found to be correlated with $L - 0.343K_{\text{sym}}$ with L and K_{sym} are evaluated at $\rho = 0.1 \text{ fm}^{-3}$.^{12, 13} It is quite unclear, why some of the investigations yield strong correlations between P_t and the various symmetry energy parameters, while, the lack of such correlations are found in other studies. In order to understand

better the dependence of the core-crust transition properties on the model used or on the various symmetry energy parameters, it is highly desirable to use different models, with their parameters varied systematically¹⁴ to yield wide variations in the properties of symmetric and asymmetric nuclear matter.

In the present work, we investigate the correlations between core-crust transition properties and the density dependence of the nuclear symmetry energy for the NS matter using three different families of extended relativistic mean-field (ERMF) model. We consider several parameterizations for each of the families of the models which were obtained by systematic variations in such way that they yield wide variations in the values of a_{sym} and its slope parameter L at the saturation density.^{15,16} The ERMF model includes the contributions from self- and mixed-interaction terms for isoscalar-scalar σ , isoscalar-vector ω and isovector-vector ρ mesons up to the quartic order.^{15,17} The presence of $\sigma - \rho$ and $\omega - \rho$ mixed interaction terms might alter the correlation of various core-crust transition properties to the density dependence of the nuclear symmetry energy. Such investigations are not performed previously in detail.⁹⁻¹² The transition density is calculated using the relativistic random phase approximation (RPA) method. For sake of comparison, we also present some results for core-crust transition density and the corresponding pressure obtained by commonly used RMF parameter sets such as NL3, FSU, GM1 and TM1. We also compare our results with those obtained from dynamical and thermo-dynamical methods.

This paper is organized as follows. In Sec 2, we present the method to calculate the ρ_t . The brief review of ERMF model is given in Sec. 3. In Sec. 4 we discuss in some detail the choices for the different families of the systematically varied ERMF models. The results obtained for the core-crust transition properties using different families of the ERMF models are presented in Sec. 5. Finally, main conclusions are drawn in Sec. 6.

2. CORE-CRUST TRANSITION

Determination of the ρ_t of the star is not easy task in general due to a very complicated structure of the star inner crust. However, the critical density at which the uniform matter of NS matter becomes unstable to a small density fluctuation at low densities, can be used as a good approximation for ρ_t of NS. There are 3 methods used widely in literature to study the instability due to small density fluctuations in low density matter. These are, the thermo-dynamical method,^{9,11,12,18-20} the relativistic,²¹⁻²³ non-relativistic^{11,12,24-26} dynamical methods and the RPA method based on Green function formalism.²⁷⁻³⁰ The thermo-dynamical method requires matter to fulfill not only the mechanical but also the chemical stability condi-

4 *A. Sulaksono, Naosad Alam and B. K. Agrawal*

tions:^{11,18}

$$\begin{aligned} -\left(\frac{\partial P}{\partial v}\right)_\mu &> 0 \\ -\left(\frac{\partial \mu}{\partial q_c}\right)_v &> 0, \end{aligned} \quad (1)$$

where v and q_c are the volume and charge per baryon number, while P is the pressure and $\mu = \mu_n - \mu_p$ is the difference between chemical potentials for the neutrons and protons. Otherwise, the matter becomes unstable. For dynamical models, the instability region of matter can be located by examining when the convexity of the free-energy curvature matrix is violated.^{21,22,24-26} It was shown by Xu *et. al*¹¹ that the thermodynamic stability is the limit of the non-relativistic dynamical model as $k \rightarrow 0$ (long-wavelength limit) when the Coulomb interaction is neglected. The relativistic RPA method, requires longitudinal dielectric functions $\varepsilon_L > 0$ when time component of four momentum $q_0 = 0$ to ensure the stability conditions at low-density region. On the other hand, it was known for some times^{21,22} that instabilities predicted by the relativistic dynamical method within Landau-Vlasov formalism is indeed equivalent to those of relativistic RPA method.

In this work, we choose relativistic RPA method to calculate core-crust transition density and pressure of NS matter. Based on this method, the transition from the core to inner crust in the NS matter takes place at the largest density for which the following condition has a solution²⁹

$$\varepsilon_L = \det [1 - D_L(q)\Pi_L(q, q_0 = 0)] \leq 0. \quad (2)$$

In Eq. (2) q_0 is the time component of the four-momentum transfer $q^\mu = (q_0, \vec{q})$ and $q = |\vec{q}|$. The explicit form of each element in the longitudinal meson propagator and longitudinal polarization matrices $D_L(q)$ and Π_L can be seen in Refs.^{29,31,32} Note, in addition to standard γ , ω , σ and ρ propagators, the matrix $D_L(q)$ contains the contributions from mixed propagators due to the presences of nonlinear mixed-interaction terms between various mesons in the ERMF model. These propagators are determined from the quadratic fluctuations around the static solutions that are generated by the second derivatives of the energy density of matter.^{31,32}

3. EXTENDED RELATIVISTIC MEAN-FIELD MODEL

We consider the NS matter which are composed of nucleons in β equilibrium. The dense matter in the core of the NS matters can be described by an effective Lagrangian density for the nucleons interacting through the exchange of σ , ω and ρ mesons. The leptons, as required to fulfill the β -equilibrium and charge neutrality conditions, are assumed to be non-interacting. The Lagrangian density for the ERMF model can be written as

$$\mathcal{L} = \mathcal{L}^{\text{lin}} + \mathcal{L}_{\text{std}}^{\text{nl}} + \mathcal{L}_{\text{mix}}^{\text{nl}} + \mathcal{L}_L. \quad (3)$$

where the

$$\begin{aligned}
\mathcal{L}^{\text{lin}} = & \sum_{J=n,p} \bar{\Psi}_J [i\gamma^\mu \partial_\mu - (M - g_\sigma \sigma) \\
& - (g_\omega \gamma^\mu \omega_\mu + \frac{1}{2} g_\rho \gamma^\mu \tau \cdot \rho_\mu)] \Psi_J + \frac{1}{2} (\partial_\mu \sigma \partial^\mu \sigma - m_\sigma^2 \sigma^2) \\
& - \frac{1}{4} \omega_{\mu\nu} \omega^{\mu\nu} + \frac{1}{2} m_\omega^2 \omega_\mu \omega^\mu - \frac{1}{4} \rho_{\mu\nu} \rho^{\mu\nu} + \frac{1}{2} m_\rho^2 \rho_\mu \rho^\mu,
\end{aligned} \tag{4}$$

is a function of the kinetic terms of nucleons; σ , ω and ρ mesons; and the corresponding linear interaction terms of nucleons. The ERMF model is introduced for the first time by Furnstahl *et al.*³³ The Lagrangian densities for non-linear self interaction terms which are usually used in standard RMF model can be written as

$$\begin{aligned}
\mathcal{L}_{std}^{\text{nl}} = & -\frac{\kappa_3}{6M} g_\sigma m_\sigma^2 \sigma^3 - \frac{\kappa_4}{24M^2} g_\sigma^2 m_\sigma^2 \sigma^4 \\
& + \frac{1}{24} \zeta_0 g_\omega^2 (\omega_\mu \omega^\mu)^2,
\end{aligned} \tag{5}$$

where σ , ω and ρ are the mesons field while g_σ , g_ω and g_ρ are their corresponding coupling constants. m_σ , m_ω , m_ρ and M are the masses for σ , ω , ρ and nucleons respectively. κ_3 , κ_4 , ζ_0 are the standard non-linear self interaction parameters. The first two terms in Eq. (5) were introduced for the first time by Boguta-Bodmer.³⁴ Inclusion of these terms provide more quantitative description of nuclear matter and finite nuclei properties than those predicted by simple linear RMF model. One of the significant effects produced by this terms in nuclear matter is softening the nuclear incompressibility. However, in general, the incompressibility predicted by standard RMF model depends sensitively also on the choice of fitting protocol and observable. For example, NL3³⁵ predicts larger but NL-Z2³⁶ smaller incompressibility compared to the experimental value.^{37,38} From theoretical point of view, the positive value of κ_4 is more favorable, otherwise the energy spectrum has no lower bound and instabilities in nuclear matter equation of state (EOS) and finite systems may occur.^{30,39} The third term in Eq. (5) was introduced by Sugahara-Toki⁴⁰ to overcome this problem. At high density, the quartic vector isoscalar nonlinear parameter ζ_0 has effect to bring down the vector potential and makes the EOS softer^{39,41} and this term plays also crucial role for transversal stability of nuclear matter due to particle hole excitations.³⁰ However, in standard RMF model, too large and unnatural value of ζ_0 can not be avoided to reach acceptable soft SNM EOS. It is reported that by tuning the ζ_0 one can generate different limiting neutron-star masses without too much modifying the behavior of the EOS around ρ_0 .^{42,43} It is worthwhile to note that isovector sector of standard RMF model relies only on just a single coupling constant g_ρ , which is usually fixed by the binding energies of asymmetric nuclei. This leaves no way to adjust the isovector properties, like, neutron-skin thickness in ²⁰⁸Pb nucleus. Any attempt to adjust the parameters of

6 *A. Sulaksono, Naosad Alam and B. K. Agrawal*

the standard RMF model to accommodate various iso-vector observables may require compromise with the quality of the fit to the well known bulk properties of the finite nuclei. The contributions of $\omega - \rho$ mixed interaction, as given by fourth term in Eq. (6), makes the RMF model more flexible.²⁸ The ERMF model contains some additional mixed interaction terms which are as follows,

$$\begin{aligned} \mathcal{L}_{mix}^{nlin} = & \frac{\eta_1}{2M} g_\sigma m_\omega^2 \sigma(\omega_\mu \omega^\mu) + \frac{\eta_2}{4M^2} g_\sigma^2 m_\omega^2 \sigma^2(\omega_\mu \omega^\mu) \\ & + \frac{\eta_\rho}{2M} g_\sigma m_\rho^2 \sigma(\rho_\mu \rho^\mu) + \frac{\eta_{1\rho}}{4M^2} g_\sigma^2 m_\rho^2 \sigma^2(\rho_\mu \rho^\mu) \\ & + \frac{\eta_{2\rho}}{4M^2} g_\omega^2 m_\rho^2 (\omega_\mu \omega^\mu)(\rho_\nu \rho^\nu), \end{aligned} \quad (6)$$

where η_1, η_2 are the nonlinear isoscalar mixed-interaction parameters while $\eta_\rho, \eta_{1\rho}$ and $\eta_{2\rho}$ are the nonlinear isovector mixed-interaction parameters. The presence of nonzero η_1 and η_2 parameters in ERMF model provides more freedom to adjust the ζ_0 into the desired value but still retain the positiveness of κ_4 .^{39,41} The presence of $\eta_\rho, \eta_{1\rho}$ and $\eta_{2\rho}$ in this model provides more freedom for controlling behavior of the EOS of asymmetric nuclear matter not only at high but also at low densities. In-particular, this nonlinear mixed-interaction terms enable one to vary the density dependence of the symmetry energy coefficient and the neutron skin thickness in finite nuclei over a wide range without affecting too much the other properties of finite nuclei.^{2,15,44} The contributions of the ρ meson self-coupling is not included in the present work. It affects the properties of the asymmetric nuclear matter only marginally, because, the expectation value of the ρ meson field is orders of magnitude smaller than those of other mesons involved.^{15,17} The last term of Eq. (3) \mathcal{L}_L is the Lagrangian density for non-interacting leptons which can be written as,

$$\mathcal{L}_L = \sum_{l=e^-, \mu^-, \nu_e, \bar{\nu}_\mu} \bar{\Psi}_l [i\gamma^\mu \partial_\mu - M_l] \Psi_l. \quad (7)$$

4. Choice for the systematically varied parameterizations

We study the core-crust transition density and the corresponding pressure in the NS for the three different families of the ERMF models obtained in Ref.¹⁶ These different families correspond to different choices of the coupling strength, ζ_0 , for the self-interaction of the ω -mesons (Eq. (5)). The value of ζ_0 were considered to be $\zeta_0 = 0.0, 0.03g_\omega^2$ and $0.06g_\omega^2$. For each of the family, the remaining parameters of the model were systematically varied to yield different values of the neutron-skin thickness in ^{208}Pb nucleus.^{15,16} In other words, for a given ζ_0 , the remaining parameter of the model were optimized using exactly same set of the protocol except for the neutron-skin thickness in ^{208}Pb . The fitting protocol comprised of the experimental data for the total binding energies and charge rms radii for many closed shell normal and exotic nuclei.¹⁶ The value of neutron-skin thickness in ^{208}Pb nucleus was also considered one of the fit data. The value of neutron-skin thickness in ^{208}Pb was

varied over a wide range of $0.16 - 0.28$ fm as it is not yet well constrained. In total, there are twenty-one parameter sets, seven parameter sets for each of the families of the ERMF model corresponding to different values of neutron-skin thickness in ^{208}Pb . These parameter sets were named as BSR1, BSR2,...,BSR21.^{15,16} The various properties of the symmetric nuclear matter associated with the BSR1 - BSR21 forces lie in a narrow range. For instance, the binding energy per nucleon for the symmetric nuclear matter $B/A = 16.11 \pm 0.04$ MeV, the nuclear matter incompressibility $K = 230.24 \pm 9.80$ MeV, the nucleon effective mass $M^*/M = 0.605 \pm 0.004$ and the saturation density $\rho_0 = 0.148 \pm 0.003$ fm⁻³. The quality of the fit to the bulk properties of the finite nuclei are also nearly the same for all the BSR forces; the rms errors on the total binding energy and the charge radii are 1.5 - 1.8 MeV and $0.025 - 0.04$ fm, respectively, for the nuclei considered in the fit. Hereafter, the parameter sets BSR1 - BSR7 with $\zeta_0 = 0$, BSR8 - BSR14 with $\zeta_0 = 0.03g_\omega^2$ and BSR15 - BSR21 with $\zeta_0 = 0.06g_\omega^2$, will be referred to as F1, F2 and F3 families of the ERMF models, respectively. The maximum mass for the NS for these three families of interaction lie in the range of $1.7 - 2.4 M_\odot$. The highest (lowest) values of maximum mass are obtained for F1(F3) families. The variation in the maximum mass of the neutron star across the families is predominantly due to the change in the values for the self-coupling of the ω -mesons. The maximum mass increases only by $\sim 0.03M_\odot$ is due to the change in the density dependence of the symmetry energy caused by the increase in neutron-skin thickness from 0.16 to 0.28 fm for the ^{208}Pb nucleus. As the neutron-skin thickness of ^{208}Pb nucleus is strongly correlated with the symmetry energy slope parameter,⁵ the different families of systematically varied parameterizations can be used to assess the model dependence and the symmetry energy dependence on the core-crust transition properties. For the sake of comparison, we also consider commonly used RMF parameterizations such as NL3,³⁵ FSU,⁴⁵ TM1⁴⁰ and GM1.⁴⁶ To this end, we would like to mention that the predictions for the finite nuclei and nuclear matter around saturation density for the non-linear RMF model considered here are more or less the same as those for the other variant, like, point coupling and density dependent meson exchange models.⁴⁷⁻⁴⁹ We have considered the RMF model which includes cross-coupling between various mesons and the self-coupling of ω -mesons in addition to the conventionally present cubic and quartic terms for the self-coupling of the σ -mesons. The results for such RMF models³⁹ are consistent with the trends obtained by Dirac-Brueckner-Hartree-Fock calculations at densities away from the saturation region.

5. Core-crust transition properties in NS

The values of the core-crust transition density are calculated in the present work using the RPA method as described briefly in Sec. 2. To facilitate the discussions, let us consider few definitions. The density dependent symmetry energy $a_{\text{sym}}(\rho)$,

8 *A. Sulaksono, Naosad Alam and B. K. Agrawal*

the slope parameter $L(\rho)$ and curvature parameter $K_{\text{sym}}(\rho)$ are defined as,

$$a_{\text{sym}}(\rho) = \frac{1}{2} \left. \frac{d^2 E(\rho, \delta)}{d\delta^2} \right|_{\delta=0}, \quad (8)$$

$$L(\rho) = 3\rho \frac{da_{\text{sym}}(\rho)}{d\rho}, \quad (9)$$

$$K_{\text{sym}}(\rho) = 9\rho^2 \frac{d^2 E_{\text{sym}}(\rho)}{d\rho^2}, \quad (10)$$

where, $E(\rho, \delta)$ is the energy per nucleon at a given density ρ and asymmetry $\delta = (\rho_n - \rho_p)/\rho$. We use Eq. (8) to calculate the symmetry energy, while one often employs the parabolic approximation and evaluates the symmetry energy as,

$$a_{\text{sym}}(\rho) \approx E(\rho, \delta = 1) - E(\rho, \delta = 0). \quad (11)$$

The shortcoming of using this approximation for calculating ρ_t and P_t are discussed well in literature.^{11, 50, 51} In the following discussions, the a_{sym} , L and K_{sym} denote their values at the saturation density ρ_0 , whereas, $a_{\text{sym},X}$, L_X and $K_{\text{sym},X}$ are evaluated at $\rho = 0.X \text{ fm}^{-3}$.

To determine the fractions of the particles of different species in the NS matter the following constraints are used:

- Balance equations for chemical potentials in the NS matter,

$$\begin{aligned} \mu_n &= \mu_p + \mu_e, \\ \mu_e &= \mu_\mu. \end{aligned} \quad (12)$$

- Charge neutrality

$$\rho_e + \rho_\mu = \rho_p. \quad (13)$$

- Conservation of total baryon density

$$\rho = \rho_n + \rho_p. \quad (14)$$

It is instructive to compare the core-crust transition properties calculated within the RPA method with those obtained from commonly used thermo-dynamical and dynamical methods. We plot in Fig. 1, the low density behavior for the EOS for β -equilibrated matter (lower panel) obtained using NL3, FSU, TM1 and GM1 parameterizations of the RMF model. The solid symbols mark the values of the core-crust transition density ρ_t and the corresponding pressure P_t which are obtained using dynamical (squares), thermo-dynamical (triangles) and RPA (circles) methods. The values of ρ_t and P_t calculated within the RPA method seem to be close to the ones obtained within the dynamical method. The values of ρ_t and P_t calculated using the thermo-dynamical method are somewhat higher. The values of P_t are plotted as a function of $L_1 - 0.343K_{\text{sym},1}$ in the upper panel. The dash line is taken from Ref.,¹² which is obtained by using the values of P_t calculated from dynamical method. It can be seen that our values of P_t calculated within the RPA method are more or less consistent with the linear correlation as shown by the dashed line.

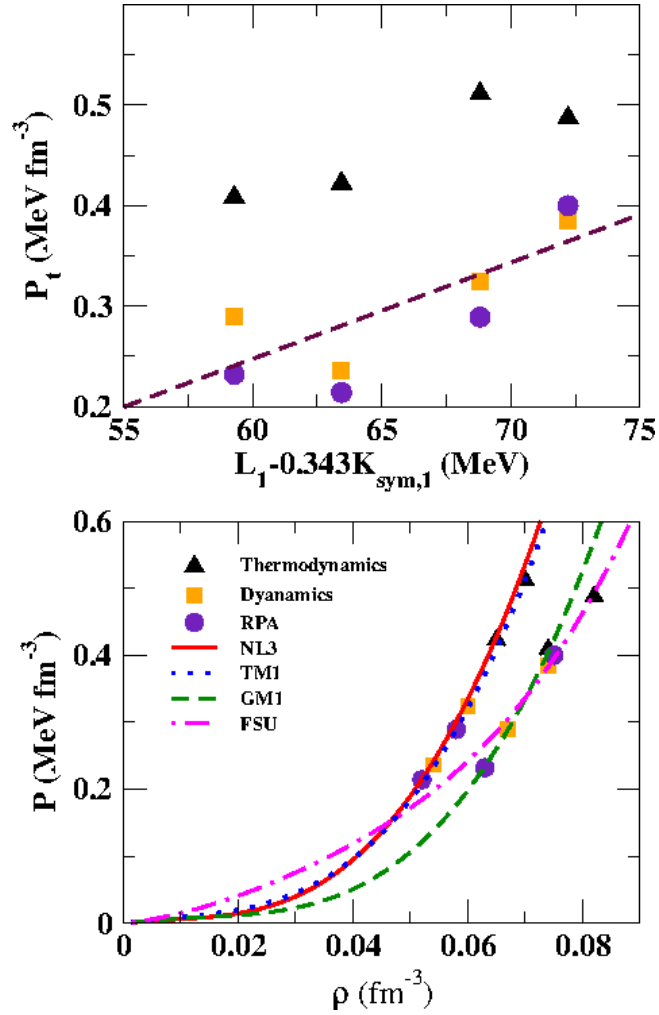


Fig. 1. Plots for the EOSs for the β -equilibrated matter obtained using the NL3, FSU, TM1 and GM1 parameterizations of the RMF model (lower panel). The filled circles represent core-crust transition density ρ_t and the corresponding pressure P_t calculated using RPA method. For the sake of comparison, the values of ρ_t and P_t obtained using thermo-dynamical (filled triangles) and dynamical methods (filled squares) of Ref.¹² are also shown. The P_t as a function of $L_1 - 0.343K_{\text{sym},1}$ are plotted in the upper panel, where, L_1 and $K_{\text{sym},1}$ represent the values of values of L and K_{sym} at $\rho = 0.01 \text{ fm}^{-3}$, respectively. The dash line is taken from Ref.¹²

Before embarking on our main results, let us look into the general trends of the density dependence of symmetry energy for the various ERMF models considered. In the left panel of Fig. 2, we plot the symmetry energy as a function of density. For the sake of completeness, the high density behaviour of $a_{\text{sym}}(\rho)$ are plotted for some selected forces from the F1, F2 and F3 families is plotted in the inset. These

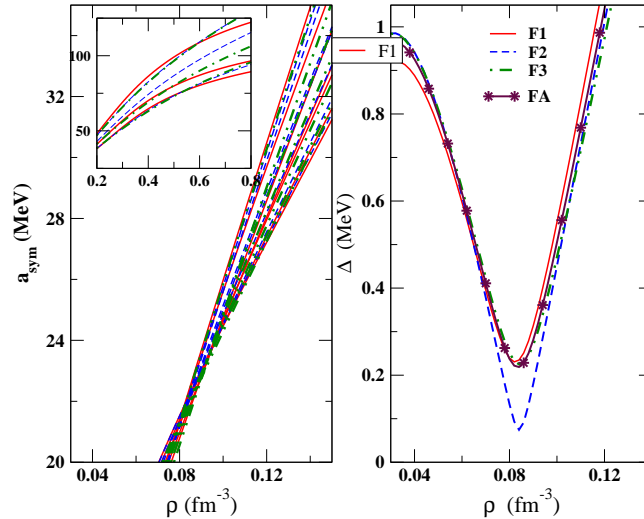


Fig. 2. The density dependence of the symmetry energy coefficient $a_{\text{sym}}(\rho)$ for various ERMF models (left panel) and the variance Δ calculated using Eq. (15) (right panel). The labels F1, F2 and F3 represent three different families of the ERMF models, whereas, FA correspond to the results obtained by combining all the three families. In the inset, the high density behaviour of $a_{\text{sym}}(\rho)$ are plotted for some selected forces from the F1, F2 and F3 families.

selected forces correspond to the neutron-skin thickness around 0.16, 0.22 and 0.28 fm in ^{208}Pb nucleus. The variance Δ for $a_{\text{sym}}(\rho)$ is plotted in the right panel. The labels $F1$, $F2$ and $F3$ denote three different families, while, FA corresponds to the results obtained by combining all the three families. The values of a_{sym} at densities in the range of $0.08 - 0.09$ fm $^{-3}$ seems to be more or less same for all the different models. The variance Δ at a given density is obtained using,

$$\Delta^2 = \frac{1}{n} \sum (a_{\text{sym}}(\rho) - \bar{a}_{\text{sym}}(\rho))^2 \quad (15)$$

where, n is the number of models and $\bar{a}_{\text{sym}}(\rho)$ is the average value at a density ρ . The variance has a minimum at $\rho \approx 0.08$ fm $^{-3}$ which is smaller than 0.11 fm $^{-3}$ as obtained for a set of SHF and RMF forces.¹²

We now consider the core-crust transition properties obtained using three different families of the ERMF models. In Fig. 3, we display the low density behavior of the EOS for β -equilibrated matter for these ERMF models. For the sake of clarity we plot the results only for a few selected forces for each of the families. The dotted lines correspond to the results for the BSR1, BSR8 and BSR15 forces belonging to the F1 (red), F2 (blue) and F3 (green) families. Likewise, the dashed correspond to BSR4, BSR11, BSR18 and solid lines are for BSR7, BSR14, BSR21. All the dotted, dashed and solid lines correspond to the forces associated with the neutron-skin thickness in ^{208}Pb to be around 0.16, 0.22 and 0.28 fm, respectively. At low densities, $\rho \sim 0.03$ fm $^{-3}$, the behavior of the EOS is more or less independent of the

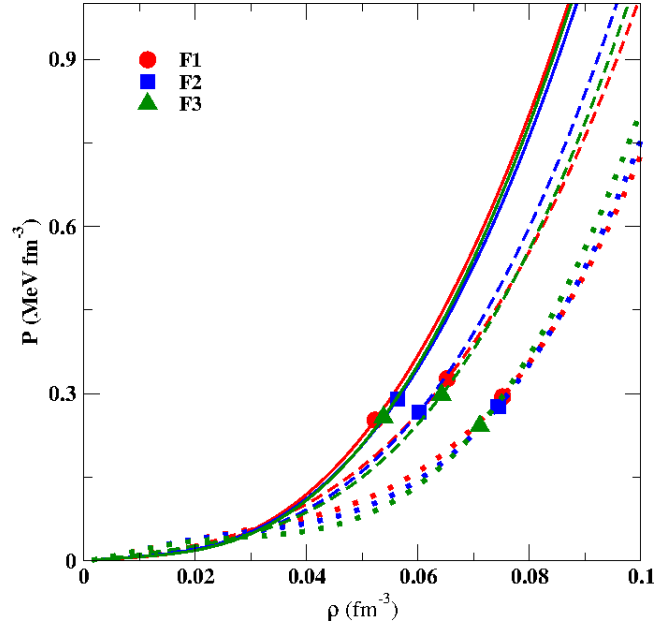


Fig. 3. Plots for the EOSs for the β -equilibrated

matter in terms of pressure versus density for the three different families of the ERMF model: F1 (red), F2 (blue) and F3 (green). The solid symbols mark the values of transition density ρ_t and the corresponding pressure P_t calculated within the RPA method. For the clarity, the results for only three forces for each of the families are plotted: BSR1, BSR8, BSR15 (dotted), BSR4, BSR11, BSR18 (dashed) and BSR7, BSR14, BSR21 (solid) lines (see text for details).

choice of the model and neutron-skin thickness in ^{208}Pb . With further increase in the density, the EOS show stronger dependence on the choice of the neutron-skin thickness. For instance, BSR1, BSR8 and BSR15 (dotted lines) correspond to the different families but have almost the similar values of a_{sym} , L and neutron-skin thickness. We see that the EOSs associated with similar neutron-skin thickness depend weakly on the choice of the families of the models. One may thus expect the values of ρ_t and P_t depend not only on the a_{sym} and L , but, also on the choice of the models. In other words, the core-crust transition properties may show some model dependence in addition to their dependence on the symmetry energy parameters a_{sym} and L .

The values of ρ_t obtained using ERMF models are shown in Fig. 4 as a function of a_{sym} (lower panel) and slope parameter L (upper panel). The values of ρ_t are correlated with the a_{sym} and L . The $\rho_t - L$ correlations is stronger than the $\rho_t - a_{\text{sym}}$ correlations. The $\rho_t - a_{\text{sym}}$ correlation is stronger within the same family. But, $\rho_t - L$ correlations are almost model independent. This is in conformity with the earlier

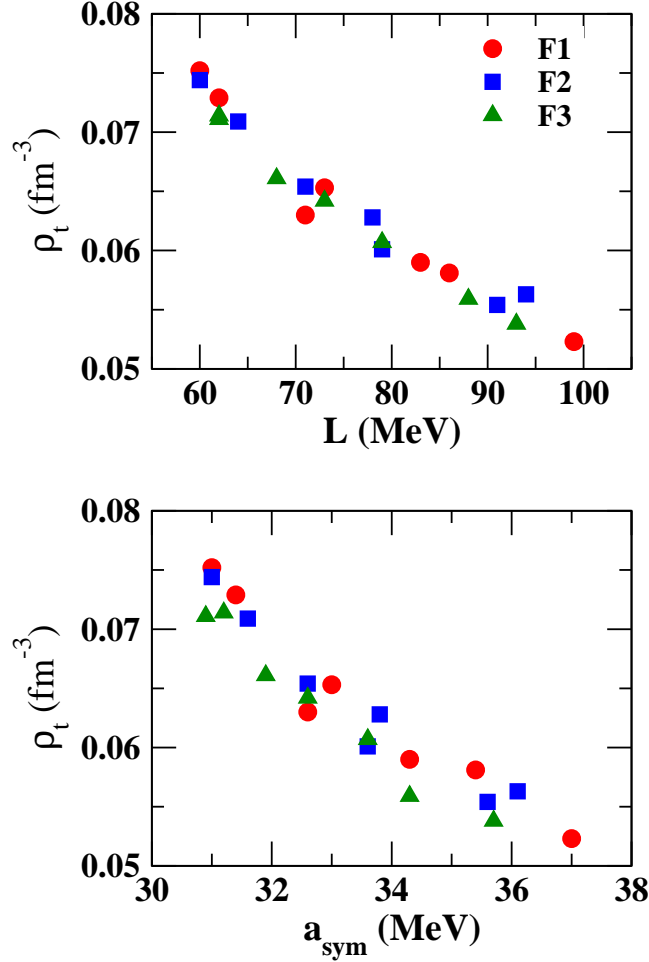


Fig. 4. Plots for the ρ_t for NS matter as a function of symmetry energy a_{sym} (lower panel) and its slope parameter L (upper panel) for 3 different families of the ERMF models.

works.^{9,12} In Fig. 5, we plot P_t for NS matter as a function of a_{sym} (lower) and L (upper) panels for the ERMF models. Our results indicate P_t is not well correlated with a_{sym} and L . Consequently, P_t is not correlated with ρ_t . For the completeness, we list the values of correlation coefficient for ρ_t and P_t with a_{sym} , L and K_{sym} in Table 1. The a_{sym} , L and K_{sym} refer to their values at the saturation density. It is little too surprising that the $P_t - L$ correlations are weak even within the same family of the ERMF model, though, the various forces within the same family differ only in the density dependence of the $a_{\text{sym}}(\rho)$. On the other hand, the calculations in Refs.^{9,10} based on a single model yield strong $P_t - L$ correlations.

We now explore the possibility of existence of strong correlations of P_t with

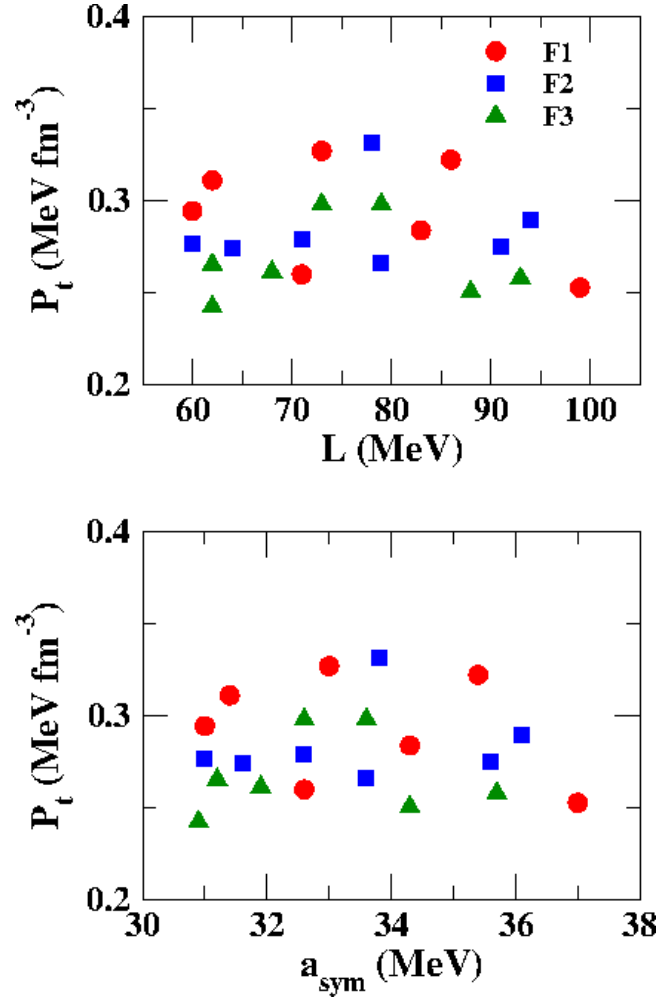


Fig. 5. Plots for the P_t , for NS matter, as a function of a_{sym} (lower panel) and L (upper panel) for 3 different families of the ERMF models.

$L(\rho)$, $K_{\text{sym}}(\rho)$ and the linear combination $L(\rho) - \alpha K_{\text{sym}}(\rho)$ at sub-saturation densities ($\rho < \rho_0$). For the quantitative assesment, the Pearson's correlation coefficients between P_t and the various symmetry energy parameters are calculated as a function of density. Pearson's correlation coefficient $C(a, b)$ for a pair of variables a and b calculated for n number of different models is given as,

$$C(a, b) = \frac{\sigma_{ab}}{\sqrt{\sigma_{aa}\sigma_{bb}}} \quad (16)$$

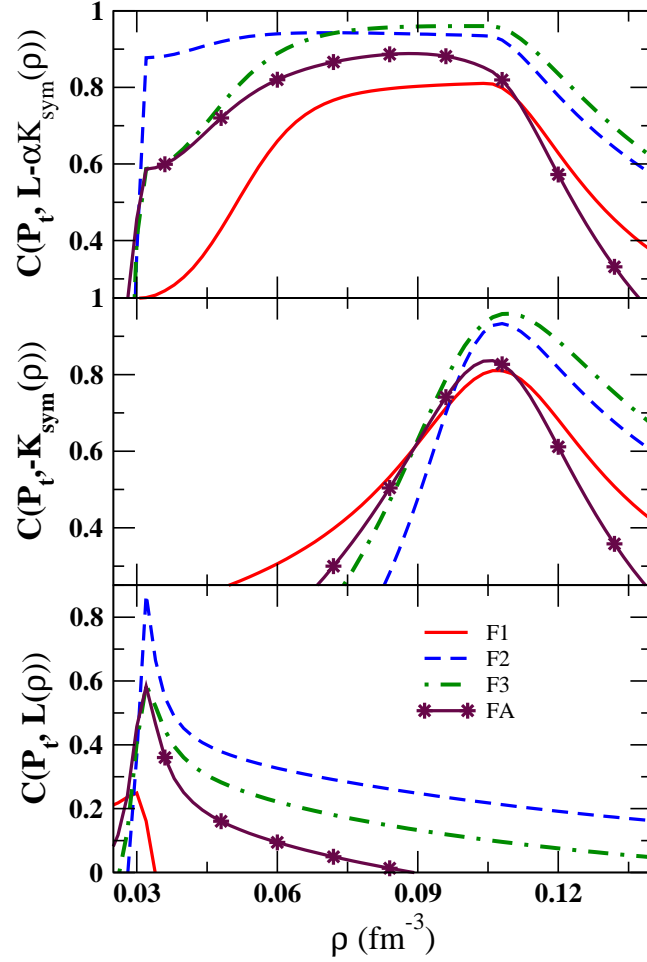


Fig. 6. The correlation coefficients for the pressure P_t with $L(\rho)$ (lower panel), $K_{\text{sym}}(\rho)$ (middle panel) and the linear combination $L(\rho) - \alpha K_{\text{sym}}(\rho)$ (upper panel) as a function of the density for 3 different families of the ERMF models.

where,

$$\sigma_{ab} = \frac{1}{n} \sum_i a_i b_i - \left(\frac{1}{n} \sum_i a_i \right) \left(\frac{1}{n} \sum_i b_i \right). \quad (17)$$

The values of $C(a, b)$ lie in the range of -1 to 1 . If $|C(a, b)| = 1$ then, the variables a and b are fully linearly correlated, whereas $C(a, b) = 0$ means, variables a and b are uncorrelated or statistically independent.

It has been suggested in Ref.¹² that P_t is reasonably correlated with the linear combination of $L(\rho)$ and $K_{\text{sym}}(\rho)$, with $\rho = 0.1 \text{ fm}^{-3}$. In Fig. 6 the correlations of P_t with $L(\rho)$ (lower), $K_{\text{sym}}(\rho)$ (middle) and $L(\rho) - \alpha K_{\text{sym}}(\rho)$ (upper panels) are

Table 1. The values of correlation coefficients $C(A, B)$ with A and B being the core-crust transition density ρ_t , corresponding pressure P_t and various symmetry energy parameters at the saturation density.

	F1	F2	F3	FA
$C(\rho_t, L)$	-0.970	-0.975	-0.994	-0.975
$C(\rho_t, a_{sym})$	-0.963	0.966	-0.985	-0.954
$C(\rho_t, K_{sym})$	0.645	0.879	0.813	0.643
$C(P_t, L)$	-0.363	0.157	0.049	-0.065
$C(P_t, a_{sym})$	-0.317	0.208	0.090	0.017
$C(P_t, K_{sym})$	-0.355	-0.545	-0.624	-0.130
$C(P_t, \rho_t)$	0.416	-0.108	-0.071	0.128

plotted as a function of density. The value of α is adjusted at a given density to maximize the correlation coefficient. The $P_t - L$ correlations are strong at quite low densities for the F2 family of the ERMF models. These correlations become weak, once the results from all the different families of the models are combined. The P_t seems reasonably correlated with $K_{sym}(\rho)$ as well as $L(\rho) - \alpha K_{sym}(\rho)$ at some sub-saturation densities. The correlation coefficient $C(P_t, -K_{sym})$ peaks at $\rho = 0.1 \text{ fm}^{-3}$, whereas, $C(P_t, L - \alpha K_{sym})$ peaks at $\rho = 0.09 \text{ fm}^{-3}$ for $\alpha = 1.31$. It is to be noted that the peaks in plots for the $C(P_t, L - \alpha K_{sym})$ verses ρ are much wider than those for the $C(P_t, -K_{sym})$ verses ρ . The strong correlations of P_t with K_{sym} at $\rho = 0.1 \text{ fm}^{-3}$ may be due the use of systematically varied models. In Fig. 7, we plot the values of P_t verses K_{sym} (lower panel) and P_t verses $L - 1.31K_{sym}$ (upper panel), the values of L and K_{sym} are evaluated at the densities for which the $C(P_t, -K_{sym})$ and $C(P_t, L - \alpha K_{sym})$ correspond to their maximum values. Our results for the correlations of P_t with the linear combination of L and K_{sym} agree only qualitatively with the ones obtained in Ref.¹² Our values for the correlation coefficient $C(P_t, L(\rho) - \alpha K_{sym}(\rho))$ is maximum at $\rho = 0.09 \text{ fm}^{-3}$, while, its value at $\rho = 0.1 \text{ fm}^{-3}$ is significantly smaller than those of Ref.¹² We also observe that the variance or the spread in the values of $a_{sym}(\rho)$ for the ERMF models considered in the present work is minimum at $\rho \sim 0.08 \text{ fm}^{-3}$ (see Fig. 2). Whereas, the variance of $a_{sym}(\rho)$ for the set of SHF and RMF forces employed in Ref.¹² is minimum around $\rho = 0.11 \text{ fm}^{-3}$. Thus, it seems that the P_t is not correlated with the symmetry energy parameters in a model independent manner.

So far we have studied the correlations of ρ_t and P_t with a_{sym} , L and K_{sym} using different families of parameterizations of the ERMF model. Each of the parameterizations were obtained by fitting exactly same set of the experimental data for the bulk properties of finite nuclei except for the neutron-skin thickness. We shall now study the variations of ρ_t and P_t with a_{sym} and $a_{sym,1}$ within a single model as it was done for DD-PC1 model.⁹ For Our investigation, we have considered the BSR1, NL3 and FSU type of functionals for the RMF model. The desired values of a_{sym} and $a_{sym,1}$ are obtained by adjusting the coupling parameters g_ρ and $\eta_{2\rho}$ appearing in Eqs. (4) and (6). In Fig. 8, we display the variations of ρ_t and P_t with

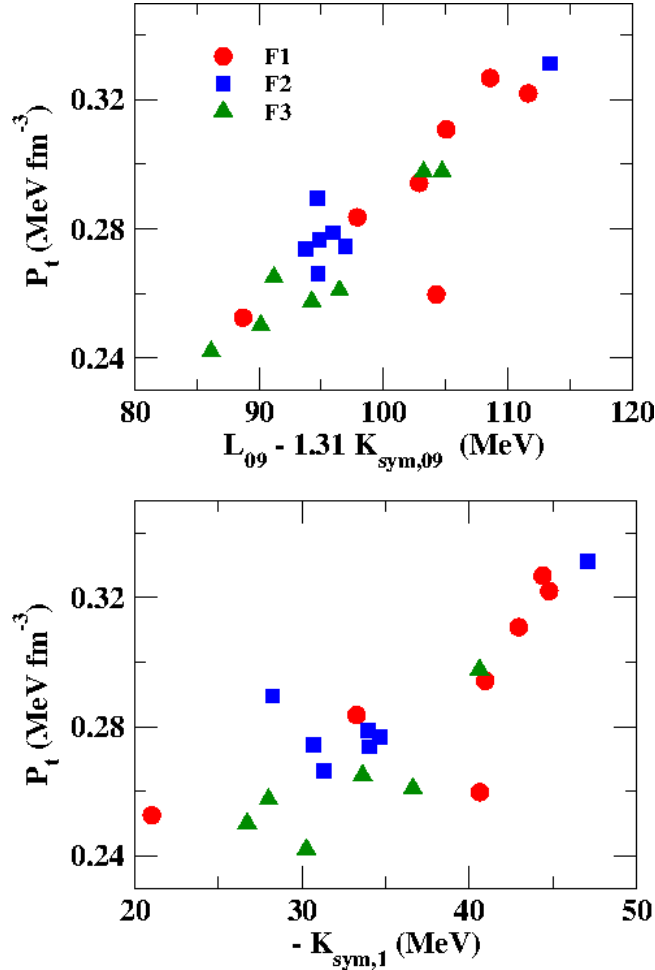


Fig. 7. Plots for the pressure, P_t , at the transition density as a function of $K_{\text{sym},1}$ (lower panel) and $L_{09} - 1.31K_{\text{sym},09}$ (upper panel) for 3 different families of the ERMF models.

$a_{\text{sym},1}$ for a fixed $a_{\text{sym}} = 32.6$ MeV for the BSR1, NL3 and FSU parameterizations. Similarly, in Fig. 9, the variations of ρ_t and P_t with a_{sym} for a fixed $a_{\text{sym},1} = 28.7$ MeV are displayed. In Table 5, we list the values of the correlation coefficient for ρ_t and P_t with a_{sym} , and $a_{\text{sym},1}$. It is evident from the Figs. 8 and 9 and Table 5 that the ρ_t is correlated with a_{sym} as well as with $a_{\text{sym},1}$, irrespective of the model used. Whereas P_t is strongly correlated only with $a_{\text{sym},1}$ in a model independent manner. The $P_t - a_{\text{sym}}$ correlations are model dependent. For instance, the value of $|C(P_t, a_{\text{sym}})| \sim 0.95$ for the BSR1 type of model which reduces to ~ 0.6 for the NL3 and FSU type of models. We can thus say once again that the pressure at the transition density is correlated with the symmetry energy parameter only at some

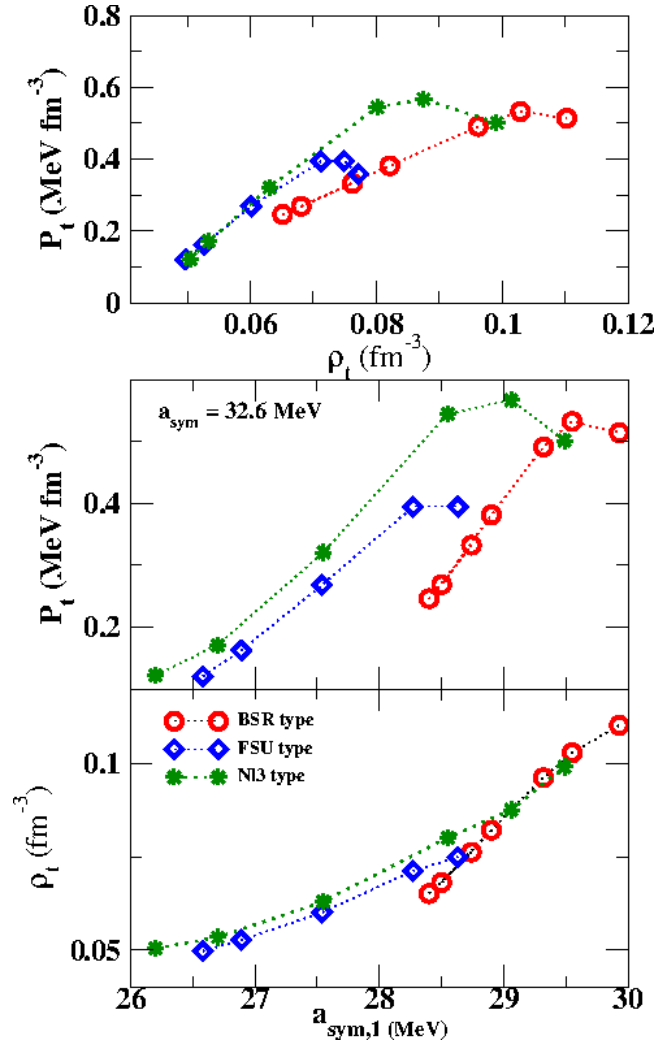


Fig. 8. Plots for the ρ_t (lower panel) and P_t (middle panel) as a function of $a_{\text{sym},1}$ and P_t versus ρ_t (upper panel) that obtained using BSR1, FSU and NL3 type functional for the RMF model. The value of $a_{\text{sym},1}$ is varied at fixed $a_{\text{sym}} = 32.6 \text{ MeV}$.

sub-saturation density. We have also repeated our calculations for the variations of ρ_t and P_t with $a_{\text{sym}}(a_{\text{sym},1})$ by fixing $a_{\text{sym},1}(a_{\text{sym}})$ to different values. The results are qualitatively the same; $P_t - a_{\text{sym}}$ correlations are model dependent.

6. Conclusions

The variations of core-crust transition properties in the neutron star with symmetry energy parameters are investigated using three different families of the systemati-

Table 2. Values for the various correlation coefficients obtained by varying a_{sym} or $a_{\text{sym},1}$ within a single model. Three different models, BSR1, FSU and NL3, are considered. The values of a_{sym} is varied by fixing $a_{\text{sym},1} = 28.7$ MeV, while, $a_{\text{sym},1}$ is varied by fixing $a_{\text{sym}} = 32.6$ MeV. The values of correlation coefficients obtained by combining the results from all the three models are presented in the last column.

	BSR1	FSU	NL3	All
$a_{\text{sym}} = 32.6$ MeV				
$C(\rho_t, a_{\text{sym},1})$	0.996	0.997	0.988	0.942
$C(P_t, a_{\text{sym},1})$	0.956	0.947	0.952	0.879
$C(P_t, \rho_t)$	0.979	0.960	0.914	0.906
$a_{\text{sym},1} = 28.7$ MeV				
$C(\rho_t, a_{\text{sym}})$	-0.995	-0.995	-0.983	-0.917
$C(P_t, a_{\text{sym}})$	-0.946	-0.659	-0.570	-0.612
$C(P_t, \rho_t)$	0.973	0.704	0.543	0.703

cally varied ERMF model. These families of the ERMF model mainly differ in the choice of the strength for the ω -meson self-coupling. Several parameterizations for each of the families are so considered that they yield wide variations in the density dependence of the symmetry energy.

Our results indicate that the transition density ρ_t is strongly correlated with the symmetry energy slope parameter L at the saturation density which is in harmony with the earlier studies.^{9,12} The ρ_t is also correlated with the symmetry energy at the saturation density, but, the correlations are marginally model dependent. The pressure P_t at the transition density, however, does not show any meaningful correlations with the values of various symmetry energy parameters at the saturation density. The possibility of existence of strong correlations between the pressure at the transition point and the symmetry energy parameters evaluated at the sub-saturation density are explored. It is found that P_t is better correlated with the curvature parameter K_{sym} alone or with the linear combination of L and K_{sym} , both the quantities calculated at some sub-saturation density. We observe that the density $\rho = 0.09 \text{ fm}^{-3}$ at which the correlation coefficient $C(P_t, L(\rho) - \alpha K_{\text{sym}}(\rho))$ peaks is quite close to the one at which the variance of $a_{\text{sym}}(\rho)$ is minimum. The strong correlations between P_t and linear combination of $L(\rho)$ and $K_{\text{sym}}(\rho)$ at $\rho = 0.1 \text{ fm}^{-3}$ for a set of SHF and RMF models¹² for which the variance of $a_{\text{sym}}(\rho)$ is minimum at $\rho = 0.11 \text{ fm}^{-3}$ also supports our observation. Though, the pressure at the transition point is correlated with linear combination of the symmetry energy slope and the curvature parameters evaluated at a sub-saturation density, such correlations show some degree of model dependence.

We also study the dependence of core-crust transition properties on various symmetry energy parameters using a single model. In this case, the symmetry energy parameters are varied by modifying the values of the model parameters around their optimal values. Two different kinds of variations in the symmetry energy pa-

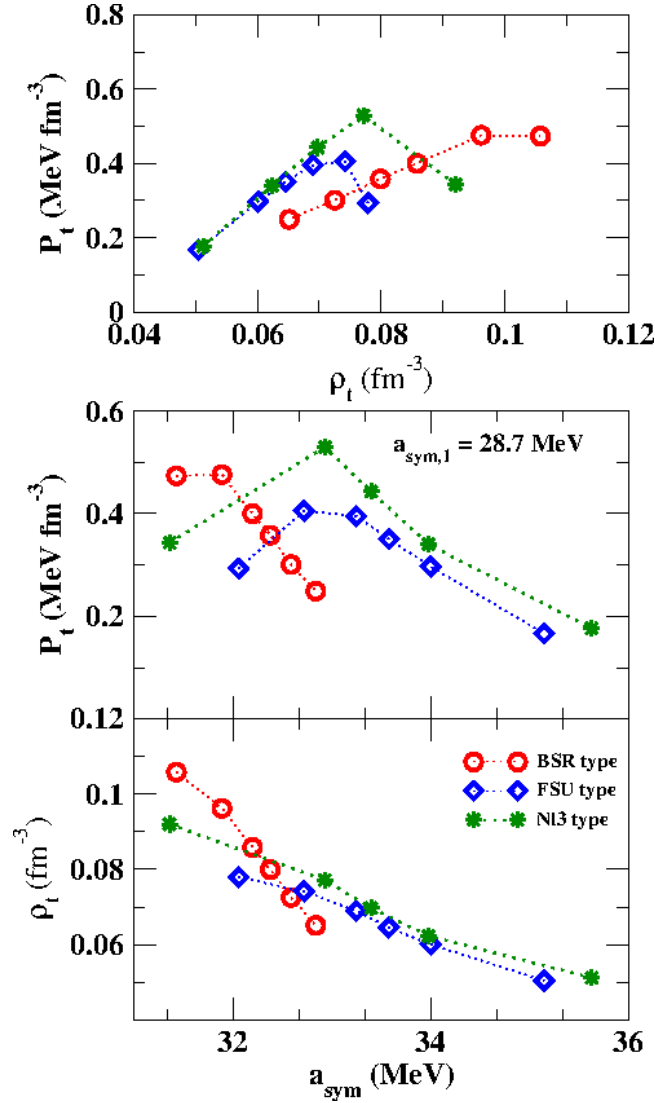


Fig. 9. Same as that of 8, but, a_{sym} is varied at fixed $a_{\text{sym},1} = 28.7 \text{ MeV}$.

parameter a_{sym} are considered. The values of a_{sym} are varied at the saturation density by keeping its value fixed at the density $\rho = 0.1 \text{ fm}^{-3}$. Another type of variations in a_{sym} is obtained by changing its value at the density $\rho = 0.1 \text{ fm}^{-3}$, but, keeping it fixed at the saturation density. The calculations are performed for the BSR1, NL3 and FSU type of the RMF model. The transition density is found to be strongly correlated with the values of a_{sym} calculated at the saturation density as well as those at $\rho = 0.1 \text{ fm}^{-3}$, irrespective of the model used. The pressure at the transition

20 A. Sulaksono, Naosad Alam and B. K. Agrawal

density is correlated in the model independent manner only with the a_{sym} at the $\rho = 0.1\text{fm}^{-3}$. The correlations of pressure at the transition density with the a_{sym} at the saturation density are highly model dependent. It thus appears once again that the pressure at the transition density is at best correlated with symmetry energy parameters at some sub-saturation density.

Acknowledgements

Anto Sulaksono acknowledges the support given by Universitas Indonesia.

References

1. J. M. Lattimer and Y. Lim, *Astrophys. J* **771**, (51) 2013.
2. R. Furnstahl, *Nucl. Phys. A* **706**, (85) 2002.
3. A. W. Steiner, M. Prakash, J. Lattimer, and P. J. Ellis, *Phys. Rep.* **411**, (325) 2005.
4. M. Warda, X. Vinas, X. Roca-Maza, and M. Centelles, *Phys. Rev. C* **80**, (024316) 2009.
5. M. Centelles, X. Roca-Maza, X. Vinas, and M. Warda, *Phys. Rev. Lett* **102**, (122502) 2009.
6. J. Piekarewicz, B. K. Agrawal, G. Colo, W. Nazarewicz, N. Paar, P.-G. Reinhard, X. Roca-Maza, and D. Vretenar, *Phys. Rev. C* **85**, (041302) 2012.
7. B. K. Agrawal, J. N. De, and S. K. Samaddar, *Phys. Rev. Lett* **109**, (262501) 2012.
8. X. Roca-Maza, M. Brenna, B. K. Agrawal, P. F. Bortignon, G. Colo, Li-Gang Cao, N. Paar, and D. Vretenar, *Phys. Rev. C* **87**, (034301) 2013.
9. Ch. C. Moustakidis, T. Nikšić, G. A. Lalazissis, D. Vretenar, and P. Ring, *Phys. Rev. C* **81**, (065803) 2010.
10. F. J. Fattoyev and J. Piekarewicz, *Phys. Rev. C* **86**, (015802) 2012.
11. J. Xu, L-W. Chen, B-A. Li and H-R. Ma, *Astrophys. J* **697**, (1549) 2009.
12. C. Ducoin, J. Margueron, C. Providência, and I. Vidaña, *Phys. Rev. C* **83**, (045810) 2011.
13. W. G. Newton, M. Gearheart and Bao-An Li, *Astrophys. J. Suppl. Ser.* **204**, (9) 2013.
14. P. Klüpfel and P.-G. Reinhard and T. J. Burvenich and J. A. Maruhn *Phys. Rev. C* **79**, (034310) 2009.
15. B. K. Agrawal, *Phys. Rev. C* **81**, (034323) 2010.
16. S. K. Dhiman, R. Kumar, and B. K. Agrawal, *Phys. Rev. C* **76**, (045801) 2007.
17. A. Sulaksono and Kasmudin, *Phys. Rev. C* **80**, (054317) 2009; Kasmudin and A. Sulaksono, *Int. J. Mod. Phys. E* **20**, (1271) 2011.
18. S. Kubis, *Phys. Rev. C* **76**, (025801) 2007; *Phys. Rev. C* **70**, (065804) 2004.
19. J. M. Lattimer and M. Prakash, *Phys. Rep.* **333**, (121) 2007; *Astrophys. J* **550**, (426) 2001.
20. Bao-Ann Li, A. T. Sustich, M. Tilley and B. Zhang, *Nucl. Phys. A* **699**, (493) 2002.
21. M. Nielsen, C. Providência and J. da Providência, *Phys. Rev. C* **44**, (209) 1991.
22. C. Providência, L. Brito, S. S. Avancini, D. P. Menezes and Ph. Chomaz, *Phys. Rev. C* **73**, (025805) 2006.
23. S. S. Avancini, S. Chiacchiera, D. P. Menezes and C. Providência, *Phys. Rev. C* **82**, (055807) 2010.
24. C. J. Pethick, D. G. Ravenhall and C. P. Lorenz, *Nucl. Phys. A* **584**, (675) 1995.
25. F. Douchin and P. Haensel, *Phys. Lett. B* **485**, (107) 2000.

26. C. Ducoin, Ph. Chomaz and F. Gulminelli, *Nucl. Phys. A* **789**, (403) 2007.
27. K. Lim and C. J. Horowitz, *Nucl. Phys. A* **501**, (729) 1989.
28. C. J. Horowitz and J. Piekarewicz, *Phys. Rev. Lett* **86**, (5647) 2001.
29. J. Carriere, C. J. Horowitz, and J. Piekarewicz, *Astrophys. J* **593**, (463) 2003.
30. A. Sulaksono, T. J. Bürvenich, P.-G. Reinhard and J. A. Maruhn, *Phys. Rev. C* **79**, (044306) 2009; A. Sulaksono, T. Mart, T. J. Bürvenich and J. A. Maruhn, *Phys. Rev. C* **76**, (041301(R)) 2007.
31. A. Sulaksono and T. Mart, *Phys. Rev. C* **74**, (045806) 2006.
32. T. Mart and A. Sulaksono, *Phys. Rev. C* **78**, (025808) 2008;
33. R. J. Furnstahl, B. D. Serot and H. B. Tang, *Nucl. Phys. A* **598**, (539) 1996; *Nucl. Phys. A* **615**, (441) 1997.
34. J. Boguta and A. R. Bodmer, *Nucl. Phys. A* **292**, (413) 1977.
35. G. A. Lalazissis, J. König and P. Ring, *Phys. Rev. C* **55**, (540) 1997.
36. M. Bender, K. Rutz, P.-G. Reinhard, J. A. Maruhn and W. Greiner, *Phys. Rev. C* **60**, (034304) 1999.
37. U. Garg *et al.*, *Nucl. Phys. A* **788**, (36) 2007.
38. T. Li *et al.*, *Phys. Rev. Lett* **99**, (162503) 2007.
39. M. Del Estal, M. Centelles, X. Viñas and S. K. Patra, *Phys. Rev. C* **63**, (024314) 2001.
40. Y. Sugahara and H. Toki, *Nucl. Phys. A* **579**, (557) 1994.
41. M. Del Estal, M. Centelles and X. Viñas, *Nucl. Phys. A* **650**, (443) 1999.
42. H. Mueller and B. D. Serot, *Nucl. Phys. A* **606**, (508) 1996.
43. F. J. Fattoyev and J. Piekarewicz, *Phys. Rev. C* **86**, (015802) 2012.
44. T. Sil, M. Centelles, X. Viñas and J. Piekarewicz, *Phys. Rev. C* **71**, (045502) 2005.
45. B. G. Todd-Rutel and J. Piekarewicz, *Phys. Rev. Lett* **95**, (122501) 2005.
46. N. K. Glendening and S. A. Moszkowski, *Phys. Rev. Lett* **67**, (2414) 1991.
47. S. Typel and H. H. Wolter *Nucl. Phys. A* **656**, (331) 1999.
48. D. Vretenar, G. A. Lalazissis, T. Nikšić, and P. Ring, *Eur. Phys. J. A* **25**, (555) 2005.
49. T. Bürvenich, D. G. Madland, J. A. Maruhn, and P.-G. Reinhard *Phys. Rev. C* **65**, (044308) 2002.
50. Ch. C. Moustakidis *Phys. Rev. C* **86**, (015801) 2012.
51. W. M. Seif and D. N. Basu *Phys. Rev. C* **89**, (028801) 2014.